The evolution and epidemiology of H3N2 canine influenza virus after 20 years in dogs

Brian R. Wasik[1] ![ORCID], Lambodhar Damodaran[2], Maria A. Maltepes[2], Ian E. H. Voorhees[1], Christian M. Leutenegger[3], Sandra Newbury[4], Louise H. Moncla[2], Benjamin D. Dalziel[5,6], Laura B. Goodman[7] and Colin R. Parrish[1]

[1]Baker Institute for Animal Health, Department of Microbiology and Immunology, College of Veterinary Medicine, Cornell University, Ithaca, NY, USA; [2]Department of Pathobiology, School of Veterinary Medicine, University of Pennsylvania, Philadelphia, PA, USA; [3]Antech Diagnostics, Mars Petcare, Science & Diagnostics, Fountain Valley, CA, USA; [4]Department of Medical Sciences, School of Veterinary Medicine, University of Wisconsin-Madison, Madison, WI, USA; [5]Department of Integrative Biology, Oregon State University, Corvallis, OR, USA; [6]Department of Mathematics, Oregon State University, Corvallis, OR, USA and [7]Baker Institute for Animal Health, Department of Public and Ecosystems Health, College of Veterinary Medicine, Cornell University, Ithaca, NY, USA

Abstract

The H3N2 canine influenza virus (CIV) emerged from an avian reservoir in Asia to circulate entirely among dogs for the last 20 years. The virus was first seen circulating outside Asian dog populations in 2015, in North America. Utilizing viral genomic data in addition to clinical reports and diagnostic testing data, we provide an updated analysis of the evolution and epidemiology of the virus in its canine host. CIV in dogs in North America is marked by a complex life history – including local outbreaks, regional lineage die-outs, and repeated reintroductions of the virus (with diverse genotypes) from different regions of Asia. Phylogenetic and Bayesian analysis reveal multiple CIV clades, and viruses from China have seeded recent North American outbreaks, with 2 or 3 introductions in the past 3 years. Genomic epidemiology confirms that within North America the virus spreads very rapidly among dogs in kennels and shelters in different regions – but then dies out locally. The overall epidemic therefore requires longer-distance dispersal of virus to maintain outbreaks over the long term. With a constant evolutionary rate over 20 years, CIV still appears best adapted to transmission in dense populations and has not gained properties for prolonged circulation among dogs.

![CAMBRIDGE UNIVERSITY PRESS logo]

Importance

Viruses occasionally jump into new hosts to cause epidemics and may spread widely due to the movement of humans or animals, or their viruses, with profound consequences for global health. The emergence and epidemiology of new epidemic viruses in companion animals provide a model for understanding disease dynamics and evolution. The H3N2 CIV arose from an avian virus, and infected dogs provide many opportunities for human exposure. H3N2 CIV transmission is dominated by fast-moving outbreaks within dense populations in and between animal shelters or kennels, while sustaining the epidemic likely requires the movement of the virus to more distant dog populations. Viral spread within North America appears to be sustained for a few years at a time, after which the virus dies out. The epidemiological and evolutionary dynamics of this virus in this structured host population show how an acute respiratory pathogen can emerge and spread in a new host and population.

Introduction

Influenza A viruses (IAVs) are extremely successful viral pathogens of vertebrates that are maintained within many natural bird reservoir populations that cause multiple spillovers and outbreaks in mammalian hosts [1]. IAV is an enveloped virus of the family *Orthomyxoviridae*, with a negative-sense genome arranged into eight units: PB2, PB1, PA, HA, NP, NA, M, and NS [2]. Some IAVs have overcome a variety of different host barriers to emerge as epidemic or pandemic pathogens in humans and domesticated or wild animals, including swine, horses, dogs, seals, cats, and mink [1, 3–5]. Spillovers of avian-origin IAV also frequently result in acute disease in other mammals – including humans - or domestic poultry with little or no onward transmission [6]. Within the human population, the IAV subtype H1N1 emerged around 1918 and that later underwent reassortment with additional avian strains to create the H2N2 and H3N2 subtypes [2]. The emergence of IAVs to cause epidemics in new animal hosts provides insights into the processes and principles of viral host-switching, allowing us to better understand future potential human pandemic viral emergences.

Carnivore mammals (members of the Order Carnivora), including dogs, have long been identified as being susceptible to infection by IAVs [3, 5]. This has included the observation of canine infection with seasonal human influenza strains [7–9], in addition to the successful experimental infection of dogs with a human H3N2 subtype [10]. The first sustained outbreak of an emergent canine influenza virus (CIV) occurred around 1999 after the transfer of an equine influenza subtype H3N8 to dogs. That outbreak in the USA was only recognized in 2004 [11], with the virus initially spread through much of the USA, and one lineage persisted until 2016 [12]. The epidemiology of H3N8 CIV was largely driven by transmission within and among shelters and kennels with high population turnover [13], so that viral lineages were strongly geographically clustered with outbreaks in major metropolitan areas, where the virus mostly died out in those areas in only a few months [14]. The story of H3N8 CIV suggested that the dog population structure (at least in the USA) was not ideal for influenza to sustain epidemic or endemic infections [12].

A lineage of avian-derived H3N2 emerged in dogs in eastern Asia (mainland China or Korean Peninsula) around 2004, resulting in sustained circulation that persists to the present day [15–17]. Viral sequence analysis revealed that the population quickly became separated into several geographic subclades in Asia, showing that the virus lineages circulated separately in a number of different geographic regions [17]. In early 2015, the H3N2 CIV was first identified in the North American continent as the cause of an outbreak in the USA around Chicago, Illinois [18]. That virus was initially introduced from Korea, and additional outbreaks occurred in many parts of the USA (including around Chicago and in Georgia, Alabama, and North Carolina), but those were largely controlled during early 2017 [19]. Subsequent H3N2 CIV outbreaks occurring later in 2017 among dogs in the USA were identified with a temporal gap from earlier cases and impacting independent locations, including among states in the Midwest (Minnesota, Ohio, Indiana, Kentucky) and Southeast (Florida, Georgia, North Carolina, South Carolina) [19]. In 2018, further unique outbreaks of H3N2 CIV were identified in Ontario (Canada), without clear sourcing from the neighbouring USA [20, 21]. Based on the geographic and temporal spread of these latter cases, as well as on the analysis of viral sequences, it was apparent that multiple international introductions of the H3N2 virus were involved in sparking the North American outbreaks that were seen between mid-2017 and 2018.

Viral emergence events in new hosts start with single infections resulting from spillovers, but those rarely go on to cause outbreaks or epidemics [22]. The emergence of viruses in epidemic forms is generally thought to be associated with the acquisition of host-adaptive mutations that allow better replication of the virus in the cells and tissues of the new host animal, as well as causing increased transmission [23]. These host-adaptive mutations are expected to arise quickly after transfer to the new host – likely during the first rounds of replication after spillover and the first animal-to-animal transfers [24–26]. While early selection of such mutations can be obvious shortly after the bottleneck that occurs upon transfer to the new host, later virus populations will diverge by sequence within the new host, and key adaptive changes are harder to define in the background of mutations arising from genetic drift and/or other selection pressures, including the increasing levels of host immunity [27–29].

Other factors associated with the emergence of respiratory viruses include their epidemiology and host ecology. These include the virological properties of incubation times and shedding patterns, as well as host population structures – such as heterogeneity in the host density and distribution, as well as movement or other connections between separated populations [30–32]. The human population is dense, well-connected, and globally mobile, resulting in few ecological barriers to global transmission of endemic and newly emerged respiratory pathogens, as shown by seasonal influenza dynamics and during the rapid global spread of the H1N1 pandemic in 2009 or SARS CoV-2 in 2020 [33–36]. In contrast, many other animals live in varying size groups, including smaller and isolated populations in the wild where pathogen transmission is self-limiting, large flocks or herds that allow efficient transfer at least within that population, and some animals have long-range movements, including globe-spanning migrations [1, 37, 38]. Domestication and farming of animals can also result in animals being gathered into novel population structures: large well-connected populations on farms, dense animal markets that allow many different animals to come in close contact, and other human-directed movements that allow new modes of spread and maintenance of pathogens compared to those seen in the wild populations of the same hosts [39, 40].

Companion animals such as dogs and cats have structured populations with additional features compared to those of domestic livestock. Those populations include many households with one or a few animals, as well as large and well-connected populations within kennels or animal shelters. Additional populations in some regions of the world include street animals that likely have variable levels of density and connectivity. In Africa, these complex population structures of dogs and anthropogenic effects of nearby human populations impact rabies virus (RABV) dispersal, transmission, and evolutionary dynamics [41, 42]. In the USA, dogs and cats live in close proximity to humans, so infected animals would result in high levels of exposure to humans of all ages and health status [43].

Here, we continue to examine the emergence, evolution, and epidemiology of the H3N2 canine IAV that has been circulating in its new host for 20 years and provide a detailed understanding of the processes that allowed its emergence and sustained transmission.

Results

Following emergence, H3N2 CIV has transferred repeatedly around Asia and North America and formed multiple clades

We assembled a complete phylogenetic analysis of full H3N2 CIV genomes since 2006 (Figure 1). Our dataset combines obtained sequences for this study with others in public repositories to generate a large-scale H3N2 genome data (*n* = 297, Supplementary Table S1) that revealed the global virus evolution in dogs. Initial phylogenetic analysis of each individual gene segment gave concordant results (Supplementary Figure S1), indicating that lineages did not result from extensive reassortment of the viral gene segments or exchange with other viral strains – which was further confirmed by reassortment analysis (Supplementary Figure S2). Full-genome alignments and phylogenetic analysis of H3N2 CIV reveal that virus population lineages can be classified into a series of distinct clades, which allow us to track circulation, population variants, and interconnectedness during different stages of the overall epidemic (Figure 1).

Emergent H3N2 CIV prior to 2010 showed extensive early transmission of viruses within and between China and South Korea [15, 16], along with a reported limited outbreak in Thailand [44], with more geographically distinct lineages being established in
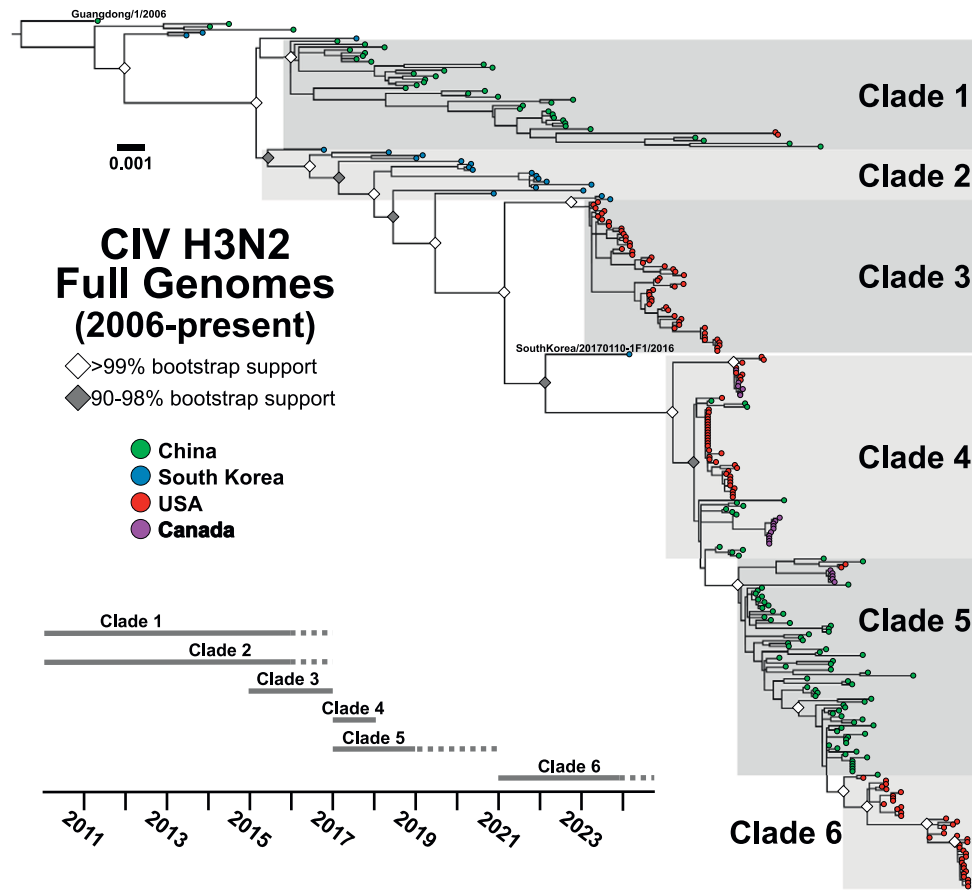
Figure 1. Overall global clade structure of H3N2 CIV genetic diversity. ML tree of the full genome data set (*n* = 297) revealing distinct early lineages and corresponding clades (shaded and labelled). Tips denote geographic sampling source (green = China, blue = Korea, red = USA, purple = Canada). The phylogeny is rooted in the sequence Guangdong/1/2006. Scale denotes nucleotide divergence. White diamonds at nodes represent bootstrap support >99%, grey is support from 90% to 98%. A general timeline of observed sampling of each clade is presented. The final Korean isolate linking Clades 2 and 4, SouthKorea/20170110-1F1/2016, is noted.

China (Clade 1) and South Korea (Clade 2). Surveys in South Korea reported fewer cases of CIV between 2016 and 2018, with the Clade 2 virus lineage likely dying out in South Korea around that time [45, 46]. Clade 1 viruses were infrequently reported in China after 2015, while CIV surveillance samples from dogs collected from 2017 to 2019 generated viral sequences that appeared to more resemble a Clade 2-derived virus that had first been circulating in South Korea. As such, a new clade (Clade 5) became established in China across several provinces, likely displacing the earlier viral lineages (Clade 1) [47–49].

The clades and lineages of North America were not derived until 2015 and show connections to several clades originating in Asia at that time (Figure 1). The first recorded introduction of H3N2 CIV into North America in early 2015 caused a series of outbreaks in the vicinity of Chicago, Illinois, and in several southeastern US states, causing a scattered set of outbreaks among dogs that continued through early 2017 [19]. Phylogenetic analysis of the viral sequences showed that the virus in US dogs was derived from a Clade 2 virus circulating in South Korea and that US lineage is herein now referred to as Clade 3 (Figure 1). Our previous study also noted that later in 2017, US outbreaks appeared in the Midwest and Southeastern states being infected by a CIV lineage distinct from Clade 3 [19]. Phylogenetic analysis of those viruses, at the time, noted a relationship to a single Clade 2 isolate in 2016 (the last CIV sample sequenced in South Korea, SouthKorea/20170110-

F1/2016) but with a sufficient branch length that made inferences of source and relatedness difficult. These secondary outbreaks of CIV in the USA formed a distinct Clade 4 (Figure 1). Our newer data also revealed multiple genetically diverse virus lineages in Clade 4 that appear to map to unique and epidemiologically disconnected outbreaks. Here, we extend on these Clade 4 viruses in the USA by analyzing a series of additional outbreaks that occurred from mid-2017 through 2018, including case clusters of genetically similar viruses in California, Florida, Ohio, and Kentucky (Figure 1). Another lineage involved infected dogs first seen in 2018 in California (near San Jose) and subsequently in New York (New York City). These Clade 4 viruses include several of the introductions seen in Ontario (Canada) [21]. In 2019, we identified a short-lived outbreak among imported dogs in quarantine in California, which did not escape into the general dog population. Those viral sequences were not of Clade 4 but showed a relationship to Clade 5 viruses observed in China (reported to be from near Shanghai) and clustered with one group of the outbreak dogs in Ontario in 2018. Further into 2019 and 2020, few cases of H3N2 CIV were reported in the USA, and the virus appeared to have died out in North America (Figure 1).

The interrelatedness of these clades and the structure of H3N2 CIV phylogenetics since roughly 2017 (Clades 4–6) suggest that the movement of viruses between Asia and North America is a hallmark of the overall epidemic.

Recent North American outbreaks of H3N2 CIV show paired epidemiology and phylogenetics

No H3N2 CIV outbreaks were reported in North America from late 2019 through 2020. There have been few reports of outbreaks in Asia, and only a single full genome H3N2 CIV sequence has been reported from China since 2019, for a virus sample collected in 2021 (with two additional HA sequences) [50]. Beginning in early 2021, an additional series of H3N2 CIV cases occurred among diverse regional outbreaks in the USA, and those appeared to be more sustained and on a larger scale relative to the outbreaks occurring in the immediately preceding years. We obtained a variety of new sequences from viral infections between 2019 and 2023 by opportunistic sampling. These covered several outbreak events, including some that appear to be ongoing at the time of preparation of this report (Supplementary Table S1). The sequence analysis showed the outbreaks to be both widely dispersed geographically and to be temporally spread out, as some viral sequence clusters were

separated by long branch lengths (Figure 1). This suggested either that we were missing key samples from our analysis or that there were gaps in the viral transmission chains with viruses being reintroduced from outside our network.

We were able to obtain USA-wide diagnostic testing case data between 2021 and early 2024, and that confirmed that our sequencing and phylogenetic analysis covered the main outbreaks that had occurred during that period (Figure 2a). Gaps in our genomic data (Figure 2b, seen as long branch lengths in the phylogeny) mostly aligned with periods of low or absent diagnostic testing positivity, suggesting those gaps did not represent major sampling omissions. The levels of testing for the different outbreaks may differ, but there appeared to be a rough concordance between the number of positive tests and the size of the outbreaks – for example, a large 2021 outbreak in Los Angeles country was represented by a large number of positive results, consistent with the County Department of Health confirmation of 1344 cases and estimates of tens of thousands of dogs being
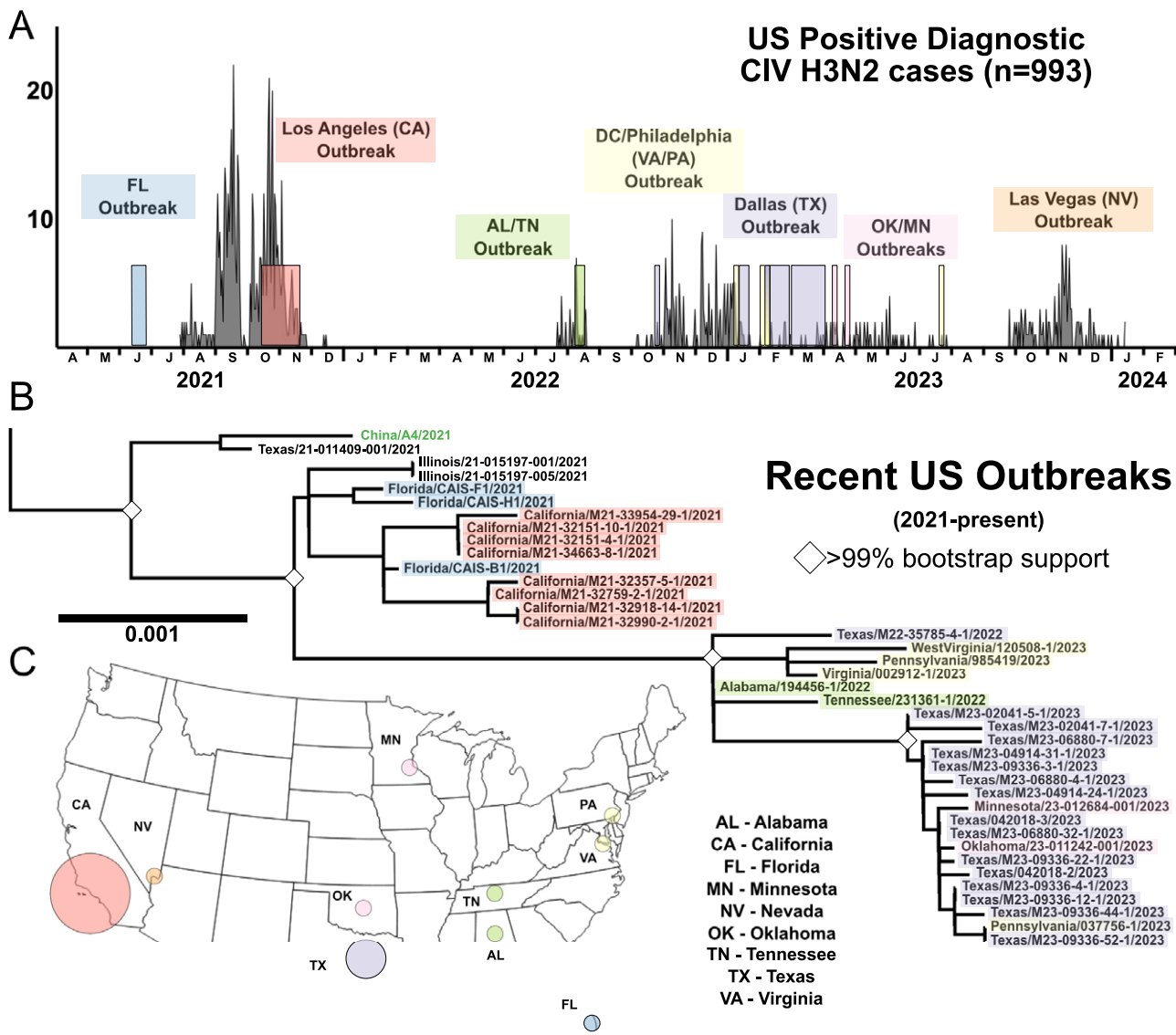

Figure 2. Recent circulation of H3N2 CIV in the USA, 2021 to present. (a) Diagnostic positive H3N2 CIV cases (*n* = 993). (b) Phylogenetics of full genomes among recent US outbreaks, with colour highlight corresponding to timeline match with diagnostic data set and geography. (c) The geography of major US outbreaks is demonstrated with colour circles corresponding to clusters in diagnostic data and phylogeny. Circles are not to scale of cases or genome count. Case data at sample geography and set to logarithmic scale are available in Figure S4.

infected (case data at scale in Supplementary Figure S4) [51]. More recent US outbreaks in late 2023 and early 2024 centred around Las Vegas, Nevada, and we do not yet have those virus samples to compare by phylogenomic analysis. Overall, these data confirm that we have captured most of the major outbreaks of the virus, as well as its natural and evolutionary history since 2021 (Figure 2).

We modelled the epidemiology of the virus over these major outbreaks using the different data available, including calculating estimates of the effective reproductive number (R) over time [52]. We used the diagnostic testing dataset obtained to infer the scope of each local outbreak (generally within a geographical area), and to make the temporal and sequence connections between the different outbreaks (Figure 3). That analysis revealed that the distinct geographical outbreaks examined experienced fluctuations in R, which may be driven in part by localized depletion of susceptible hosts – but which is also expected for a host population that shows extensive contact heterogeneity – i.e., some animals being in dense and connected populations within animal shelters and kennels, while others are dispersed and disconnected as they are living in households and have many fewer contacts with other dogs. We were able to measure three predominant geographical outbreak centres: Los Angeles, California; Dallas/Fort Worth, Texas; and Las Vegas, Nevada. In each outbreak, periods of R > 1 were measured, including periods of high transmission where the R was between 2.5 and 4. Troughs of transmission with R < 1 were also observed. The largest outbreak (Los Angeles) with the greatest data volume resulted in the best resolution with mean R measures having low error variance across the timescale, where dramatic epidemiological changes to the outbreak (September 2021) can be identified. In contrast, smaller outbreaks (in Dallas and Las Vegas) reported lower case data volume. We calculated a larger degree of error and noise in the data for those outbreaks, making distinct temporal changes in mean R values difficult to identify with confidence. Overall, the epidemiological dynamics measured were similar to the "boom and bust" patterns seen between 2015 and 2017 in the Chicago and Atlanta areas [19].

Directional transfer of H3N2 CIV between Asia and North America in recent years is a result of an increased virus population in Asia

A key question for understanding the epidemiology of the viruses in North America and Asia is the movement of viruses between those two regions, and in particular, the directionality and frequency of
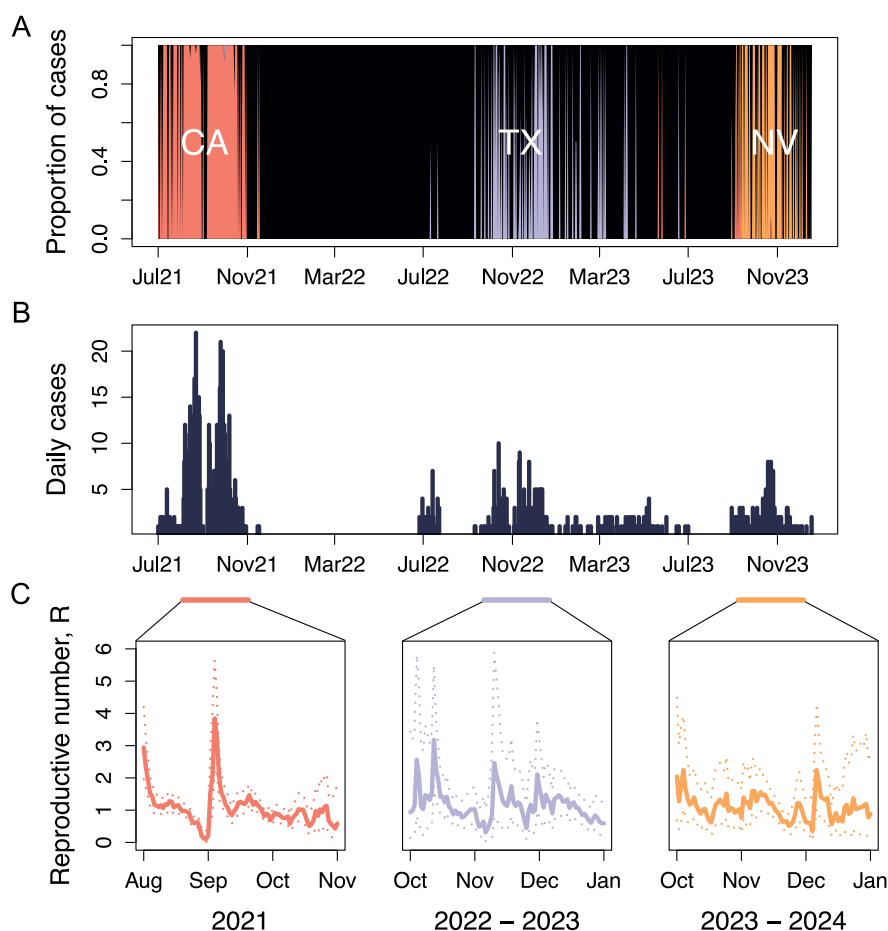

Figure 3. Epidemic dynamics of H3N2 CIV in the USA. (a) Proportion of daily cases attributed to three major outbreaks in Los Angeles, California (CA), Dallas/Fort Worth, Texas (TX), and Nevada (NV). The areas under the red (CA), blue (TX), and yellow (NV) curves represent the proportion of total cases associated with each state on a given day. (b) Daily number of new cases over time. (c) Effective reproductive number (R) estimates for each outbreak during the periods indicated by horizontal bars. Solid lines represent mean estimates, while dashed lines show the 95% credible interval of the posterior distribution.

any transfers that have occurred. To reveal the most likely routes of transfer, we tested a recent subset of the phylogenetic data (see Methods and materials, Clades 4–6) using two models: discrete trait diffusion and structured coalescent. The implementation of a discrete trait diffusion model with a Bayesian stochastic search variable selection (BSSVS) allows us to infer statistically supported rates of transition between regions across a phylogeny – i.e., showing which region is most likely seeding infections to other regions. We also used a Structured Coalescent Model to estimate the size of virus populations in each region based on their genetic diversity, and thereby inferring the region with a larger infected population. The results of both models generally agreed, inferring similar tree topologies and transmission rates between the two regions (Figure 4a and Supplementary Figure S5). Both analyses suggest five independent introductions from Asia into North America before 2021. Using the discrete trait model, we infer a higher mean rate of transitions from Asia to North America (1.4628 transitions/year, 95% HPD: [0.0332, 3.6722]) than from North America to Asia (0.4968 transitions/year, 95% HPD: [6.035E-6, 1.567]), though both transition rates had strong posterior support (posterior probability of 0.99) and a Bayes Factor support (9000).

Although discrete trait approaches are computationally tractable, they can perform poorly in the presence of biased sampling. We therefore used a structured coalescent model to independently infer virus population sizes and rates of migrations between North America and Asia. These approaches appear to more clearly model source-sink dynamics in the presence of biased sampling [53, 54], and also estimating viral effective population size (N_e) for each region, a proxy for infected population size [55]. The mean N_e in Asia was 3.4438 (95% HPD: [2.6039, 4.389]), which was significantly greater than the N_e for North America of 0.1571 (95% HPD: [0.106, 0.2162]) (Figure 4b). The higher inferred Ne matches our expectation that there is a larger virus population in Asia which acts as a source for introductions of novel lineages introduced into North America. We also estimated a backwards-in-time migration rate, which represents the rate of viruses moving to a given region A from a given region B. We estimated a higher backwards in time migration rate to North America from Asia (1.260 migrations/year, 95% HPD: [0.4474, 2.1399]) compared to the rate to Asia from North America (0.0894 migrations/year, 95% HPD [2.9079E-3, 0.2134]), consistent with the results of the discrete trait diffusion.

The rate of H3N2 CIV sequence evolution is consistent over host geography and time

To examine the temporal nature of the full genome dataset, we used well-dated samples (YYYY-MM-DD) to analyse the maximum likelihood genome phylogeny, plotting the root-to-tip length data against the sampling date (using the TempEst algorithm). That showed a consistent clock-like rate that averaged 1.76×10^{-3} substitutions/site/year ($R^2 = 0.95$) over all outbreaks across two continents, and since the emergence of H3N2 CIV in dogs around 2004 (Figure 5a). Rates of individual segments fell in a range of $1.25-2.00 \times 10^{-3}$ (Supplementary Figure S3). That consistent clock-like evolution revealed no evolutionary behaviours that might indicate pronounced selections (e.g., bursts of adaptive evolution) on the virus in either its apparent reservoir among dogs in Asia or during the outbreak spread within North America. Attempts to analyse the clock by distinct geography or timescale windows showed no noteworthy variation from the full dataset mean (data not shown).

The nucleotide substitution rate for each genome segment was further determined using a Bayesian coalescent method in BEAST. Among the H3N2 CIV segment ORFs, substitution rates were largely similar – with a higher rate for the HA gene segment (rising to significance against 5 of 7 other segments, save NA and NS1) (Figure 5b). These rates are largely similar to those seen for another influenza virus previously seen in dogs (H3N8 equine-origin CIV, analysis from Wasik et al. [12]), though higher rates were seen in H3N2 CIV among the PB1, PA and HA segments
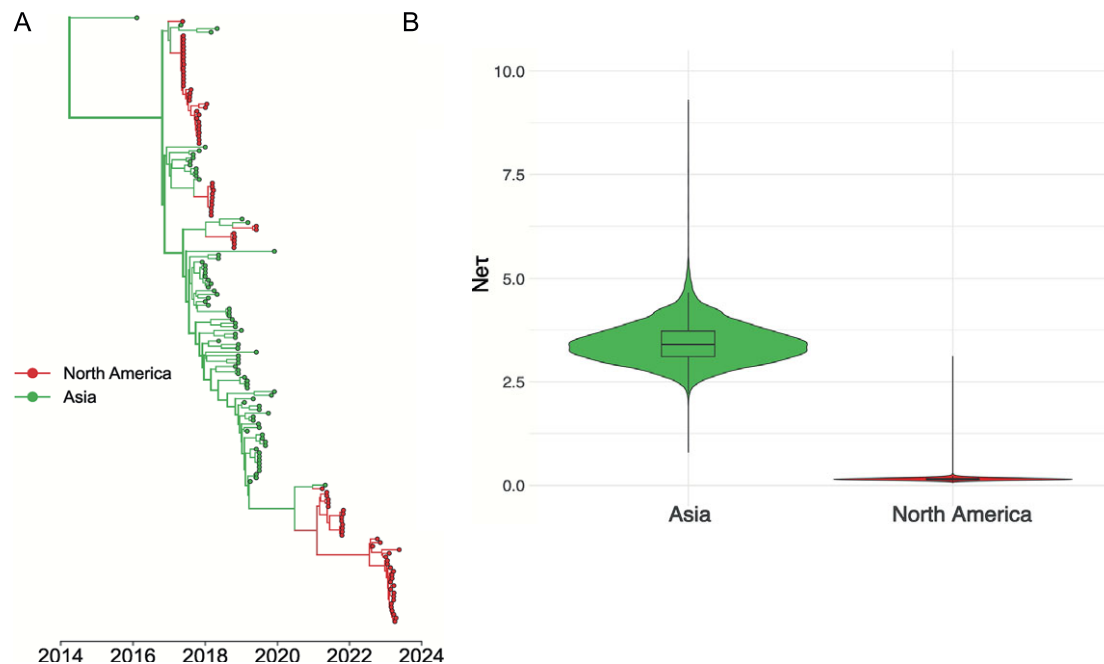

Figure 4. H3N2 CIV circulating in Asia act as viral sources for introductions into North America. (a) MCC tree from a structured coalescent analysis of recent subset H3N2 CIV genomes from North America and Asia. Nodes are coloured by their inferred geographic region; the thickness of the branches corresponds to the number of taxa that descend from the given branch. (b) Effective population size estimates for each geographic deme were estimated using MultiTypeTree v8.1.0.
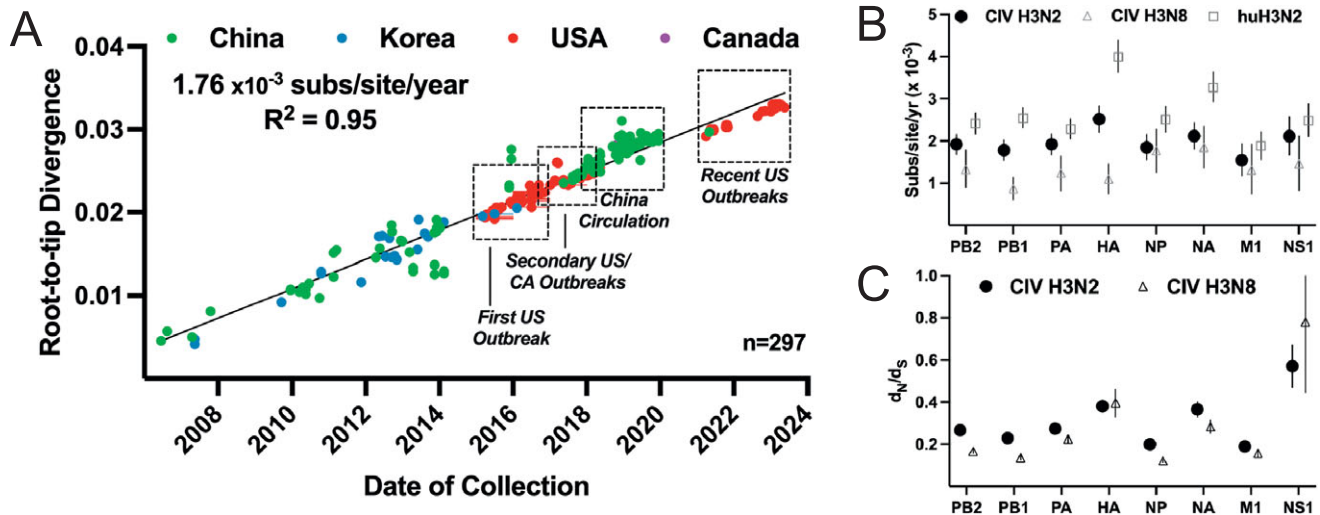
Figure 5. Temporal evolution of H3N2 CIV during continuous dog-to-dog circulation. (a) A root-to-tip analysis of H3N2 CIV full genomes, shows the divergence since the first common ancestor of the virus represented by the basal node of the phylogeny. This shows a consistent evolutionary rate of 1.76×10^{-3} substitutions/site/year. (b) Individual segment ORF substitution rates were calculated in BEAST and compared to H3N8 CIV and human seasonal H3N2. (c) Mean segment ORF d_N/d_S ratios were calculated using SLAC and compared to H3N8 CIV.

(1.782 vs. 0.87, 1.917 vs. 1.237, and 2.519 vs. 1.102, all 10^{-3} substitutions/site/year, respectively). The rates seen in both the H3N2 and H3N8 CIVs were lower in nearly all segments than those observed in seasonal H3N2 human influenza virus, with greatest pronouncement and significance relative to the HA and NA glycoproteins [56]. To generate a rough proxy of natural selection in the H3N2 CIV during the 20 years of dog-to-dog transmission, we used the model statistical method SLAC (Single-Likelihood Ancestor Counting) [57] to determine the mean d_N/d_S ratio for each segment (Figure 5c). The greatest potential signals of positive selection were seen in the HA, NA, and NS segment ORFs. The d_N/d_S ratios observed in CIV were generally higher than previous measures of H3N8 CIV (2003–2016) evolution, apart from HA and NS.

Global H3N2 CIV evolution has resulted in the cumulative fixation of non-synonymous mutations

To understand the likely functional effects of the viral evolution, we identified non-synonymous mutations that became fixed during H3N2 CIV evolution (Figures 1 and 6). Most clustered at key nodes within the phylogenetic tree, appearing following likely bottlenecks during transfers to new geographical regions. The overall evolution of the virus is re-reviewed in Figure 6, and key non-synonymous mutations that became fixed during the evolutionary pathway are highlighted. For example, 13 coding mutations became fixed within 7 of the 8 gene segments of the virus during the emergence of Clade 2 in South Korea, and additional groups of non-synonymous mutations (ranging in numbers from 3 to 15 over the entire genome) became fixed during the subsequent clade-defining events (Figure 6 and Supplementary Tables S3 and S4).

Mutations span the genome and appear in multiple functional domains of the influenza gene products. A notable fixation was the truncation of the NS1 protein at the C-terminus during Clade 4 evolution. A truncation of NS1 has previously been observed in the H3N8 subtype in horses and dogs and was related to host-specific adaptation of innate immunity [58, 59]. Several changes in PB2 (S714I) and PA (E327K and S388G) have previously been

identified during mammalian adaptation of the polymerase sub-units, related to ANP32A co-factor utilization [23, 60, 61].

H3N2 CIV evolution has included HA-specific mutations in both the head and tail domains

The HA protein controls receptor binding and cell membrane fusion, and is the major antigenic determinant of influenza, so that mutations in the HA may play key roles in controlling CIV biology and epidemiology. We identified the major fixed HA mutations of H3N2 CIV following the establishment of Clade 4 (Figure 7a and Supplementary Table S3) and mapped their position onto the HA monomer structure (Figure 7b). Following the last reported South Korean-origin genome, several nonsynonymous mutations have fixed in the HA gene of CIV lineages and clades. First, upon the establishment of Clade 4, there fixed an asparagine to aspartic acid mutation (N188D, in H3 numbering) at the top of the HA1 head near the sialic acid receptor binding site (RBS). This mutation was discussed in [47] as potentially playing a role in clade-specific phenotypes. That Clade 4 transition also fixed a stalk mutation (HA2-V89I). During Clade 5 evolution during circulation in China, two major nodes were observed in the phylogenetic analysis. Upon circulation in 2018, there fixed another HA1 mutation from valine to isoleucine (V112I). Later in 2019, there fixed both an HA1 mutation (V78I) as well as a glycine to serine change in the final residue of the signal peptide (Gsig16S). Clade 6 represents all US outbreaks after 2021 where lineages likely resulted from multiple independent introductions, therefore unique HA fixed mutations can be seen with temporal and geographic patterns (Supplementary Table S4). An HA2 mutation was seen fixed in the earliest US samples in 2021 (R82K), while an HA1 asparagine to threonine change was seen starting in 2022 viruses (N171T, in the RBS). In the most recent Clade 6 viruses in the US (2023), we observe regional subclade lineages with unique HA fixations (Figure 7). In the Mid-Atlantic region (around Washington DC and Philadelphia, Pennsylvania) viruses have an HA2 mutation (S113L) in addition to an isoleucine to methionine (I245M) change in the HA1 head near the RBS. In contrast, viruses found in the subclade around Dallas,
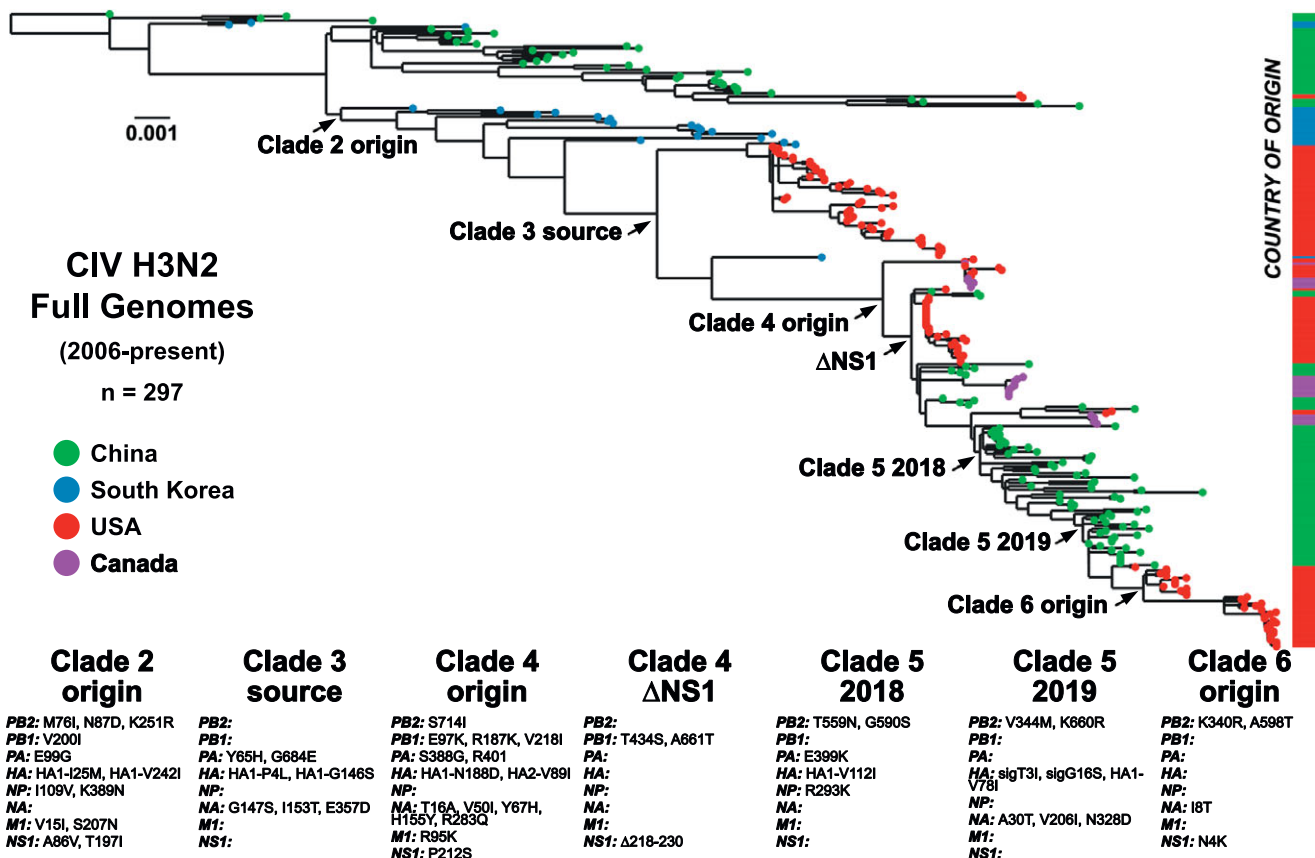
Figure 6

CIV H3N2 Full Genomes

(2006–present)

n = 297

- 🟢 China
- 🔵 South Korea
- 🔴 USA
- 🟣 Canada

Clade 2 origin
Clade 3 source
Clade 4 origin
ΔNS1
Clade 5 2018
Clade 5 2019
Clade 6 origin

0.001

COUNTRY OF ORIGIN

	Clade 2 origin	Clade 3 source	Clade 4 origin	Clade 4 ΔNS1	Clade 5 2018	Clade 5 2019	Clade 6 origin
PB2:	M76I, N87D, K251R		S714I		T559N, G590S	V344M, K660R	K340R, A598T
PB1:	V200I		E97K, R187K, V218I				
PA:	E99G	Y65H, G684E	S388G, R401		E399K		
HA:	HA1-I25M, HA1-V242I	HA1-P4L, HA1-G146S	HA1-N188D, HA2-V89I		HA1-V112I	sigT3I, sigG16S, HA1-V78I	
NP:	I109V, K389N				R293K		
NA:		G147S, I153T, E357D	T16A, V50I, Y67H, H155Y, R283Q	T434S, A661T		A30T, V206I, N328D	I8T
M1:	V15I, S207N		R95K				
NS1:	A86V, T197I		P212S	Δ218-230			N4K

Figure 6. Fixed mutations at key transitional nodes and international transfer events. (a) An ML tree of H3N2 CIV genomes with geographic sampling sources coded on tips (green = China, blue = Korea, red = USA, purple = Canada) and on the corresponding bar to the right of the tree. (b) Noted start of Clade 2, circulating in South Korea. (c) Thr transition of Clade 2 to Clade 3, international introduction of US outbreaks, 2015–2017. (d) Start of Clade 4, after last known South Korean isolate. (e) A major early genetic bottleneck of Clade 4 by NS1 truncation. (f) Early convergence in Clade 5, ~2018 circulation in China. (g) Later convergence in Clade 5, ~2019 circulation in China. (h) Start of Clade 6, with US outbreaks from 2021 to present.
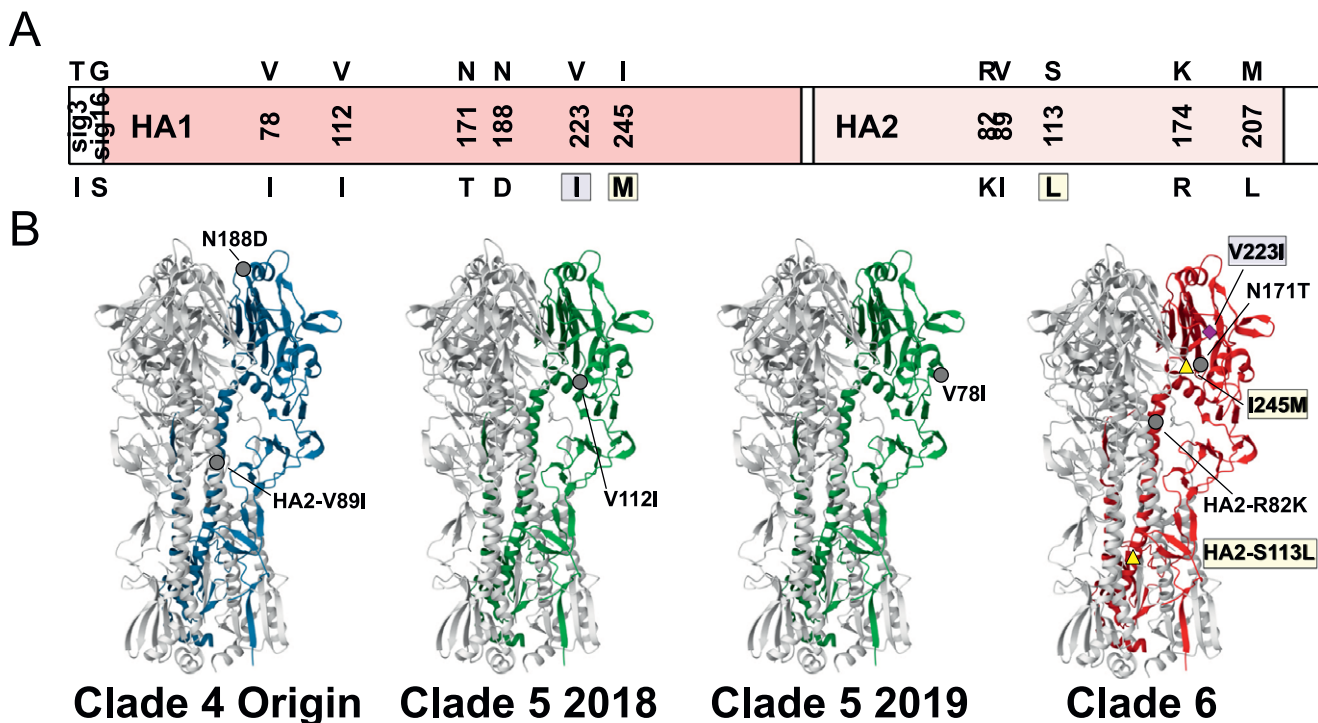
Figure 7

A

sig3	sig16	HA1	78	112	171	188	223	245	HA2	82	89	113	174	207	

Top row: T G — — V — V — — N — N — V — I | — RV — S — — K — M
Bottom row: I S — — I — I — — T — D — I — M | — KI — L — — R — L

B

Clade 4 Origin — N188D, HA2-V89I

Clade 5 2018 — V112I

Clade 5 2019 — V78I

Clade 6 — V223I, N171T, I245M, HA2-R82K, HA2-S113L

Figure 7. Recent molecular evolution of H3N2 CIV hemagglutinin. (a) Schematic of the HA ORF showing with nonsynonymous mutations fixed since the last Clade 2 isolate, SouthKorea/20170110-1F1/2016. HA1 and HA2 positions follow H3 numbering. Signal peptide sequence residues are noted as sigX. (b) The location of key HA1 and HA2 mutations on the monomer of HA, occurring during key transitions in the recent evolution of H3N2 CIV. Mutations specific to the most recent Clade 6 US subclades (Mid-Atlantic, yellow and Texas, purple) are highlighted.

Texas, contain a HA1-V223I mutation (previously observed in Clade 5) shown to increase virion thermal stability [62] and is located in a region that contains antigenic site D in human H3 viruses.

Discussion

Here, we further reveal how the H3N2 CIV emerged, evolved, and spread around the world during the 20 years that it has been circulating in dogs, providing an example of an influenza virus switching hosts to cause a sustained epidemic in a mammalian host population. Our results emphasize the interconnections between viruses circulating in different regions of Asia and those in North America. We show that around 2017, the H3N2 CIV was reduced to a single lineage that has since expanded to include viruses in mainland China, the USA and Canada. The data also strongly suggest that there were two introductions into the USA in 2021 and 2022. The first led to outbreaks during 2021 that started in Florida and then caused a large outbreak in the Los Angeles, California area that continued for several months, but which died out by the end of that year. The second introduction occurred around June or July of 2022 that resulted in a sustained outbreak in Dallas/Fort Worth, Texas, which then spread to cause a series of outbreaks in many areas of the USA, which have continued to the present (Figure 2).

Overall and recent epidemiology

The results again confirm that the epidemiology of this virus in dogs in North America is outbreak-driven and constrained by the host population structure. Consistent observations and analysis have shown that CIV (both H3N8 and H3N2) spread is characterized by rapid transmission within geographic areas among group-housed dogs in kennels, animal shelters, and day-care settings [13, 14, 19, 63]. Among recent US outbreaks of CIV, the largest and longest duration have occurred within larger metropolitan areas, where circulation has been sustained for up to several months, although all observed outbreaks ultimately died out after between 1 and about 6 months (Figure 2). The more recent CIV epidemiology was revealed by the analysis of nationwide diagnostic testing data, which showed the duration, intensity, and locations of the major outbreaks that occurred (Figures 2 and 3). That analysis was also compared to parallel phylogenetic and phylogeographic studies based on full genome sequencing data. Although both sets of data resulted from opportunistic sampling, the patterns revealed were similar, indicating that they would explain the virus spread and evolution in North America during this period.

Little recent data is available about the viruses in Asia and their circulation patterns, with only a single full H3N2 CIV sequence being available since 2019, so it is not possible to compare the details of the recent epidemiology or evolution of the viruses in Asia and North America. However, it appears that during the last several years, the viral population has been distributed between China and North America (with no virus being reported from South Korea since around 2017). Our analysis suggests a significantly greater likelihood of transmission from Asia to North America than the reverse (Figure 4). The Centers for Disease Control and Prevention has estimated that as of 2019, roughly 1.06 million dogs are imported into the USA annually [64]. This is a trend that has increased since the 2020 COVID pandemic [65, 66], while screening for infectious respiratory diseases in imported dogs is minimal [67].

The effective reproduction number (R) for the H3N2 CIV was estimated from the data and varied widely depending on the structure of the dog population. Within the large metropolitan centres, the R was between 1 and 4, mainly due to the rapid and sustained spread of the virus within more densely housed dogs. It is assumed that within each population outbreak, recovered animals would become resistant due to the development of protective immunity, so without the addition of large numbers of new susceptible animals, the Susceptible-Infected-Recovered (SIR) dynamic would apply, and the virus would die out naturally. While there is a H3N2-specific canine vaccine which can protect dogs from severe disease, we lack data on the use of vaccines, or on the vaccine status of dogs in case and outbreak settings. While administration of vaccination well in advance of virus introduction would likely reduce or stop transmission, vaccination in the face of ongoing outbreaks is unlikely to affect the dynamics of viral spread as incubation and transmission is likely more rapid than the development of vaccine-induced immunity [63]. Having the vaccination status of dogs in outbreak settings known in future studies would allow the role of prophylactic vaccination to be better understood.

A common prediction is that transmission of a virus in a new host will select for host-adaptive mutations which would result in more efficient infection, replication, and transmission – often referred to as 'gain-of-function' mutations. While the H3N2 CIV has acquired many changes with the potential to be host-adaptive during its thousands of exclusively dog-to-dog infections and transmissions, we do not yet see clear evidence of CIV being able to spread more effectively in dogs within dense populations or gaining an increased ability to transfer between geographically separate population centres.

H3N2 CIV evolution and possible host adaptation

The H3N2 CIV has likely undergone over 1000 exclusively dog-to-dog infections and transfers since it emerged, and there has been a linear acquisition of genetic change since 2005. While some adaptive changes likely arose during the first series of transfers of the H3N2 CIVs in dogs, those are difficult to define as the sequence of the directly ancestral avian virus is not known [17]. The evolution of the virus included several clades that appear to have been established through single bottleneck events which may be due to epidemiological events. We therefore cannot determine which mutations were under positive selection which resulted in their fixation, versus neutral or even deleterious mutations that were fixed during the bottlenecks.

While several mutations in H3N2 CIV are in viral genes and proteins associated with host adaptation in other influenza spillovers (Supplementary Tables S3 and S4), we do not have clear evidence that those have resulted in gain of function for the virus [47, 68]. In other studies small numbers of experimental passages in ferrets were sufficient to make high pathogenicity H5N1 influenza viruses more transmissible in that new host [69, 70], while for SARS CoV-2 several variants that show increased transmission in humans have arisen during the first years of spread in humans in the face of rising immunity [71–74]. A possible explanation for the

apparent lack of gain of function for H3N2 CIV is that the complex environmental pressures of the canine population may be constraining the viral evolution, since most spread and infections have occurred in dense populations of animals in close contact, but which result in SIR-mediated die outs. Mutations selected in those host populations would therefore differ from those that would favour the long-distance transfers between population centres required to sustain long-term transmission. Properties that may favour the second type of spread might include persistent infections, prolonged shedding, virus stability, and fomite-mediated transfer, as suggested by the life-history trade-off evolutionary theory [75].

Are H3N2 CIVs a risk to humans and might those risks be changing?

The risk of emergence of the H3N2 CIV into additional mammalian hosts (including humans) is a concern, but currently, the threat is unknown. While swine have often been proposed to be intermediate host that allows influenza viruses to jump onward into humans to cause sustained epidemics on at least a few occasions ("mixing vessels"), other mammalian-adapted influenza viruses (in horses, seals, cows, mink) have so far not been the origin of human epidemics [3, 76, 77]. The changes in the H3N2 CIV have included previously identified mammalian-adaptive sites [23], some experimentally confirmed as having biological effects [47], and the H3N2 CIV appears to have lost the host range for at least some avian hosts [78]. Other concerning adaptive changes that underlie known human adaptation and pandemic risk (including NP changes to evade MxA/BTN3A3 restriction factors, and HA RBS changes to the 226/228 residues) are absent, as the H3N2 CIV remains 'avian-like' [79–81]. Changes have occurred in NA domains related to ligand binding, but the constellation of changes does not include any known inhibitor-resistance markers, suggesting antiviral use in zoonotic exposure would be efficacious [82].

Cross-species transmission of H3N2 CIV into cats has occurred in Korea and the USA [83, 84]. In a serosurvey of racehorses in China, some riding club horses were positive for H3N2 CIV, positivity being strongly associated with exposure to dogs [85]. To date, no natural human infections with either H3N8 or H3N2 CIV have been reported. Following the 2015 US outbreak of H3N2 CIV, a human spillover risk assessment was performed on a Clade 3 isolate, examining for receptor utilization, replication kinetics in human cells, and antibody cross-reactivity, and concluded that H3N2 CIV posed a low risk for human populations [68].

Besides point mutations, reassortments of influenza viruses allow the mixing of viruses to find favourable genetic combinations [86, 87]. No reassortant influenza viruses were seen in dogs in the USA (Supplementary Figures S1 and S2). H3N2 CIV reassortants with human, swine, and avian influenza viruses have been reported in Korea and China [88–91], but none have generated sustained transmission chain lineages and the fitness effects for either dogs or humans are unknown. While the H3N8 and H3N2 CIVs both circulated in dogs in the USA during 2015 and 2016, the two strains were not found within the same population so no recombinant opportunities likely occurred [12, 19]. The lack of reassortant viruses in North American dogs suggests differences in host population ecology or epidemiology of the CIV and the other viruses leading to fewer mixed infections. It is unknown whether additional viral strains, including high pathogenicity avian influenza (HPAIV) H5N1 clade 2.3.4.4b may create reassortant events, but additional screening of domestic animals for influenza viruses is likely warranted [92–95].

Overall conclusions

Respiratory viruses emerging to cause human pandemics readily spread through host populations, crossing oceans within days and overwhelming control measures [33, 96, 97]. Here, we show that emerging epidemic diseases in animal populations may differ significantly from those seen in humans, even though the transmission potential for each virus is similar. The different outcomes are mostly due to the different population structures and interconnectedness of different wild or domesticated animals [13]. There are around 900 million domestic dogs worldwide, and many live in very close proximity to their human owners, allowing for high levels of human exposure [43]. While the H3N2 CIV has circulated widely in Asia and North America, and undergone several transfers between those regions, it has not been reported from Europe, Australia, Africa, or other regions with large dog populations and veterinary disease testing. The relatively unrestricted import of large numbers of rescued dogs from Korea and China to the USA may have facilitated the repeated introduction of the virus. The movement of CIV-infected dogs from the USA or Canada (or from Asia) to Europe, Australia, or other places around the globe seems less likely. The H3N2 CIV has repeatedly died out in North America, and the H3N8 CIV also died out in North American dogs in 2017 with little directed intervention [12, 19]. This indicates that modest interventions such as animal symptom screening, quarantine, and slowing the movement of infected dogs would allow the H3N2 CIV to be eradicated from the dog population, while increased testing or quarantine of imported dogs would likely prevent the virus from being re-introduced. The epidemiological and evolutionary patterns seen here may also prove a useful comparison with influenza viruses in other hosts – horses, swine, mink, seals, and cows – where interventions at key points could also result in them being controlled or eradicated.

Methods and materials

H3N2 sample collection

Virus samples were obtained from various diagnostic centres, including the Animal Health Diagnostic Center (Cornell University College of Veterinary Medicine), Wisconsin Veterinary Diagnostic Laboratory (University of Wisconsin School of Veterinary Medicine), and Antech Diagnostics. These samples followed from routine passive diagnostic testing for respiratory disease in dogs (listed in Supplementary Table S1, red). Samples were received as either nasal or pharyngeal swab material or extracted total nucleic acid (tNA) first utilized for quantitative reverse transcription-PCR (qRT-PCR) positivity. Two additional samples were first isolated in embryonated chicken eggs or MDCK cells for virus isolation (noted in Supplementary Table S1). Viral RNA (vRNA) was extracted from clinical swab samples and virus isolation using the QIAamp Viral RNA Mini kit. Purified vRNA or tNA was then either directly used for influenza multi-segment RT-PCR or stored at −80°C.

Generation of influenza viral sequences

Virus genomes from samples were generated as cDNAs using a whole genome multi-segment RT-PCR modified from the Zhou et al. CDC protocol, described previously and repeated here in full [12, 98]. A common set of primers (5′ to 3′, uni12a, GTTACGCGC-CAGCAAAAGCAGG; uni12b, GTTACGCGCCAGCGAAAG-CAGG; uni13, GTTACGCGCCAGTAGAAACAAGG) that

recognize the terminal sequences of the influenza A segments were used in a single reaction with SuperScript III OneStep RT-PCR with Platinum *Taq* DNA polymerase (Invitrogen). Following confirmation by gel electrophoresis, viral cDNA was purified either by standard PCR reaction desalting columns or with a 0.45× volume of AMPure XP beads (Beckman Coulter). Libraries were generated either by Nextera XT with 1 ng of cDNA material or Nextera FLEX with 150–200 ng (Invitrogen). Libraries were multiplexed, pooled, and sequenced using Illumina MiSeq 2 × 250 sequencing. As most samples were isolated from direct nasal swabs and may contain intra-host viral diversity at sequencing depth, raw reads were deposited in the Sequence Read Archive (SRA) at NCBI.

Consensus sequence editing was performed using Geneious Prime. Paired reads were trimmed using BBduk script (https://jgi.doe.gov/data-and-tools/bbtools/bb-tools-user-guide/bbduk-guide/) and merged. Each sequence was assembled by mapping to a reference sequence of a previously annotated H3N2 isolate (A/canine/Illinois/41915/2015(H3N2)). Consensus positions had read depth > 300 and > 75% identity.

Diagnostic testing data and R estimation

Diagnostic qRT-PCR tests positive for H3N2 CIV (*n* = 993) were obtained, spanning from 2021 July 27 to 2024 January 12, identifying cases in 17 US states by zip code. R estimation from daily case data followed the standard methodology described in [52]. The generation time was assumed to follow a discretized version of a gamma distribution with a mean of 3.5 days and a variance of 2 days. The temporal window over which R was assumed constant was 7 days.

Phylogenetic analysis

H3N2 CIV nucleotide sequences were downloaded from the NCBI Influenza Virus Database and were compiled with generated consensus genomes for this study and organized in Geneious Prime. We examined the larger database collection of H3N2 present in dog hosts for both inter- and intra-subtype reassortants using RDP4 (seven methods: RDP, GENECONV, Bootscan, MaxChi, Chimaera, SiScan, 3seq) and excluded those found to be a statistically significant outlier in two or more methods [99]. The dataset with full genome coverage (*n* = 297) is provided in Supplementary Table S1. Sequences were manually trimmed to their major open reading frames (PB2: 2280 nt, PB1: 2274 nt, PA: 2151 nt, HA: 1701 nt, NP: 1497 nt, NA: 1410 nt, M1: 759 nt, and NS1: 654-693 nt) and either analyzed separately or concatenated with all other genome segments from the same virus sample. Nucleotide sequences were aligned by MUSCLE [100] in the Geneious Prime platform. Maximum likelihood (ML) phylogenetic analysis was performed by either PhyML or IQ Tree [101, 102], employing a general time-reversable (GTR) substitution model, gamma-distributed (Γ4) rate variation among sites, and bootstrap resampling (1000 replications). ML trees were visualized and annotated using FigTree v1.4.4 (tree.bio.ed.ac.uk/software/figtree/). An additional reassortment analysis for all 297 aligned H3N2 CIV sequences was performed using Treesort [103]. Reassortment events were inferred on each branch of the phylogeny using HA as the fixed reference tree.

The temporal signal was assessed by a regression root-to-tip genetic distance against the date of sampling using our ML tree and the TempEst v.1.5.3 software [104]. Accurate collection dating to the day (YYYY-MM-DD) was utilized for all samples where this information was available. Sampling dates used for all isolates are listed in Supplementary Table S1.

Bayesian phylodynamic analysis

We used a Bayesian coalescent approach to better estimate our phylogenetic relationships, divergence times, and population dynamics. Analyses were performed in BEAST v.1.10.4 [105], where Markov chain Monte Carlo (MCMC) sampling was performed with a strict clock, a GTR substitution rate with gamma distribution in four categories (Γ4), set for temporal normalization by sample collection date (YYYY-MM-DD to best accuracy), and assuming a Bayesian Skyline Plot (BSP) prior demographic model. Analyses were performed for a minimum of 100 M events, with replicates combined in Log Combiner v1.10.4. Outputs were examined for statistical convergence in Tracer v1.7.2 (effective sample size [ESS] ≥200, consistent traces, removed burn-in at 10%–15%) [106].

For the discrete trait diffusion model [107] and the structured coalescent model [108], we used a subset of diverged lineage genomes (*n* = 169) starting with the last Korean isolate (SouthKorea/20170110-1F1/2016) in Clade 2 and related lineages in Clades 4, 5, and 6. This dataset was annotated for two geographic locations (Asia or North America) based on sample collection. These annotations for the geographic region were used as discrete traits for discrete trait diffusion modelling and as demes for structured coalescent modelling. We first performed a discrete trait diffusion model for the sequences using BEAST v1.10.4. We used an HKY nucleotide substitution model with gamma-distributed rate variation among sites, a lognormal relaxed clock model, and a GMRF skyride model [109–111]. We ran six independent MCMC chains of 50 million steps, logging every 5000 steps. Outputs were examined for statistical convergence in Tracer v1.7.2 (ESS ≥200, consistent traces, removed burn-in at 10%). The three runs with the highest ESS values were selected and combined using LogCombiner v1.10.4. The last 500 posterior-sampled trees from the combined runs were used as an empirical tree set to perform discrete trait diffusion analysis. We performed an ancestral state reconstruction to determine the discrete trait states across all branches of the phylogeny. We used the BSSVS method to estimate the most parsimonious asymmetric rate matrix between discrete traits [107]. We used a Poisson mean prior to 1 non-zero rate. The Bayes factor support for the rates was calculated using SpreaD3 v0.9.7.1 [112]. The maximum clade credibility (MCC) tree was summarized with the program TreeAnnotator v1.10.4 using the combined tree files for the runs with the highest ESS value using a posterior sample of 10000 trees. The structured coalescent analysis was implemented using the MultiTypeTree v 8.1.0 package available in BEAST v2.7.6 [113]. These models estimate an effective population size (N_e) in each deme, and asymmetric migration rates between demes [108]. We calculate the asymmetric migration rates as 'backwards-in-time' rates, which parameterize the rate of movement of ancestral tree lineages between demes backwards in time. This represents the probabilities per unit time of individual members of a particular deme having just transitioned from some other deme. We also calculate the 'forwards-in-time' rates, which parameterize the (constant) probability per unit time that an individual in some deme will transition to a new deme. The relationship between the backwards and forwards migration rates is given by:

$$B_{ij} = F_{ji} * (N_j / N_i)$$

where B_{ij} is the backwards-in-time rate from deme i to deme j, F_{ij} is the forwards-in-time rate from deme i to deme j, and where N_i and N_j are the effective population sizes of these two demes [53]. We used an asymmetric model of migration with a lognormal prior distribution for the rate with a mean of 1 and upper limit of 20 as well as a uniform prior distribution for the Log Population size tau (Effective population size) between 0.001 and 10000. We ran six independent MCMC chains of 100 million steps, logging every 10000 steps. Run convergence was assessed using Tracer 1.7.2 (ESS ≥200, consistent traces, removed burn-in 10%). The three runs with the highest ESS values across parameters were combined using LogCombiner v1.10.4. The MCC tree was summarized for the tree files of the three runs with the highest ESS using the program TreeAnnotator v1.10.4 for a posterior sample of 10000 trees. Visualization for MCC trees was achieved using the BALTIC python package (https://github.com/evogytis/baltic). Branches of the phylogenies were coloured based on annotations for the most probable ancestral state or deme for the MCC tree of the discrete trait diffusion model analysis and structured coalescent analysis respectively.

Analysis of selection pressures

The relative numbers of synonymous (d_S) and nonsynonymous (d_N) nucleotide substitutions per site in each ORF of each segment were analysed for the signature of positive selection (i.e., adaptive evolution, $p < 0.05$ or > 0.95 posterior) using SLAC (**S**ingle-**L**ikelihood **A**ncestor **C**ounting) within the Datamonkey package (datamonkey.org/; [57]).

Hemagglutinin structural modelling

HA structures and positions of CIV mutations were visualized in Mol* from the RCSB Protein Database (PDB). The structure of A/HongKong/1/1968 (4FNK) was used as an H3 model.

Graphing and statistical analysis

Graphs in Figures 2 and 5 were generated in GraphPad Prism v.10. Figure 3 was generated by R version 4.2.3 without the use of any additional packages.

References

[1] **Yoon S-W**, **Webby RJ and Webster RG** (2014) Evolution and ecology of influenza a viruses. *Current Topics in Microbiology and Immunology* **385**, 359–375.

[2] **Krammer F**, et al. (2018) Influenza. *Nature Reviews. Disease Primers* **4**, 3.

[3] **Parrish CR**, **Murcia PR and Holmes EC** (2015) Influenza virus reservoirs and intermediate hosts: Dogs, horses, and new possibilities for influenza virus exposure of humans. *Journal of Virology* **89**, 2990–2994.

[4] **Runstadler JA**, **Puryear W.** A brief introduction to influenza a virus in marine mammals. *Methods in Molecular Biology (Clifton, N.J.)* 2020; **2123**: 429–450.

[5] **Wasik BR**, **Voorhees IEH and Parrish CR** (2021) Canine and feline influenza. *Cold Spring Harbor Perspectives in Medicine* **11**, a038562.

[6] **Reperant LA**, **Rimmelzwaan GF and Kuiken T** (2009) Avian influenza viruses in mammals. *Revue Scientifique Et Technique (International Office of Epizootics)* **28**, 137–159.

[7] **Kilbourne ED and Kehoe JM** (1975) Demonstration of antibodies to both hemagglutinin and neuraminidase antigens of H3N2 influenza a virus in domestic dogs. *Intervirology* **6**, 315–318.

[8] **Seiler BM**, et al. (2010) Antibodies to influenza a virus (H1 and H3) in companion animals in Iowa, USA. *The Veterinary Record* **167**, 705–707.

[9] **Yin X**, et al. (2014) Serological report of pandemic and seasonal human influenza virus infection in dogs in southern China. *Archives of Virology* **159**, 2877–2882.

[10] **Paniker CK and Nair CM** (1972) Experimental infection of animals with influenzavirus types a and B. *Bulletin of the World Health Organization* **47**, 461–463.

[11] **Crawford PC**, et al. (2005) Transmission of equine influenza virus to dogs. *Science (New York, N.Y.)* **310**, 482–485.

[12] **Wasik BR**, et al. (2023) Understanding the divergent evolution and epidemiology of H3N8 influenza viruses in dogs and horses. *Virus Evolution* **9**, vead052.

[13] **Dalziel BD**, et al. (2014) Contact heterogeneity, rather than transmission efficiency, limits the emergence and spread of canine influenza virus. *PLoS Pathogens* **10**, e1004455.

[14] **Hayward JJ**, et al. (2010) Microevolution of canine influenza virus in shelters and its molecular epidemiology in the United States. *Journal of Virology* **84**, 12636–12645.

[15] **Li S**, et al. (2010) Avian-origin H3N2 canine influenza a viruses in southern China. *Infection, Genetics and Evolution: Journal of Molecular Epidemiology and Evolutionary Genetics in Infectious Diseases* **10**, 1286–1288.

[16] **Song D**, et al. (2008) Transmission of avian influenza virus (H3N2) to dogs. *Emerging Infectious Diseases* **14**, 741–746.

[17] **Zhu H**, **Hughes J and Murcia PR** (2015) Origins and evolutionary dynamics of H3N2 canine influenza virus. *Journal of Virology* **89**, 5406–5418.

[18] **Voorhees IEH**, et al. (2017) Spread of canine influenza a(H3N2) virus, United States. *Emerging Infectious Diseases* **23**, 1950–1957.

[19] **Voorhees IEH**, et al. (2018) Multiple incursions and recurrent epidemic fade-out of H3N2 canine influenza a virus in the United States. *Journal of Virology* **92**: e00323–18.

[20] **Weese JS**, et al. (2019) Emergence and containment of canine influenza virus a(H3N2), Ontario, Canada, 2017–2018. *Emerging Infectious Diseases* **25**, 1810–1816.

[21] **Xu W**, et al. (2020) Phylogenetic inference of H3N2 canine influenza a outbreak in Ontario, Canada in 2018. *Scientific Reports* **10**, 6309.

[22] **Wasik BR**, et al. (2019) Onward transmission of viruses: How do viruses emerge to cause epidemics after spillover? *Philosophical transactions of the Royal Society of London. Series B, Biological Sciences* **374**, 20190017.

[23] **Long JS**, et al. (2019) Host and viral determinants of influenza a virus species specificity. *Nature Reviews. Microbiology* **17**, 67–81.

[24] **Antia R**, et al. (2003) The role of evolution in the emergence of infectious diseases. *Nature* **426**, 658–661.

[25] **Pepin KM**, et al. (2010) Identifying genetic markers of adaptation for surveillance of viral host jumps. *Nature Reviews. Microbiology* **8**, 802–813.

[26] **Rochman ND**, **Wolf YI and Koonin EV** (2022) Molecular adaptations during viral epidemics. *EMBO Reports* **23**, e55393.

[27] **Carabelli AM**, et al. (2023) SARS-CoV-2 variant biology: Immune escape, transmission and fitness. *Nature Reviews Microbiology* **21**, 1–16.

[28] **Su YCF**, et al. (2015) Phylodynamics of H1N1/2009 influenza reveals the transition from host adaptation to immune-driven selection. *Nature Communications* **6**, 7952.

[29] **Tamuri AU**, et al. (2009) Identifying changes in selective constraints: Host shifts in influenza. *PLoS Computational Biology* **5**, e1000564.

[30] **Anderson RM and May RM** (1991) *Infectious Diseases of Humans: Dynamics and Control*. Oxford University Press.

[31] **Gandon S**, et al. (2016) Forecasting epidemiological and evolutionary dynamics of infectious diseases. *Trends in Ecology & Evolution* **31**, 776–788.

[32] **Plowright RK**, et al. (2017) Pathways to zoonotic spillover. *Nature Reviews. Microbiology* **15**, 502–510.

[33] **Bedford T**, et al. (2020) Cryptic transmission of SARS-CoV-2 in Washington state. *Science (New York, N.Y.)* **370**, 571–575.

[34] **Hernandez MM**, et al. (2021) Molecular evidence of SARS-CoV-2 in New York before the first pandemic wave. *Nature Communications* **12**, 3463.

[35] **Lemey P**, et al. (2014) Unifying viral genetics and human transportation data to predict the global transmission dynamics of human influenza H3N2. *PLoS Pathogens* **10**, e1003932.

[36] **Tegally H**, et al. (2023) Dispersal patterns and influence of air travel during the global expansion of SARS-CoV-2 variants of concern. *Cell* **186**: 3277–3290.e16.

[37] **Fourment M**, **Darling AE and Holmes EC** (2017) The impact of migratory flyways on the spread of avian influenza virus in North America. *BMC Evolutionary Biology* **17**, 118.

[38] **Olsen B**, et al. (2006) Global patterns of influenza a virus in wild birds. *Science (New York, N.Y.* **312**, 384–388.

[39] **Nelson MI**, et al. (2015) Global migration of influenza a viruses in swine. *Nature Communications* **6**, 6696.

[40] **Sievers BL**, et al. (2024) 'Smart markets': Harnessing the potential of new technologies for endemic and emerging infectious disease surveillance in traditional food markets. *Journal of Virology* **98**, e0168323.

[41] **Mancy R**, et al. Rabies shows how scale of transmission can enable acute infections to persist at low prevalence. *Science (New York, N.Y.)* 2022; **376**: 512–516.

[42] **Talbi C**, et al. (2010) Phylodynamics and human-mediated dispersal of a zoonotic virus. *PLoS Pathogens* **6**, e1001166.

[43] **Schmidt PL** (2009) Companion animals as sentinels for public health. *The Veterinary Clinics of North America. Small Animal Practice* **39**, 241–250.

[44] **Bunpapong N**, et al. (2014) Genetic characterization of canine influenza a virus (H3N2) in Thailand. *Virus Genes* **48**, 56–63.

[45] **Lee C-Y** (2023) Evolution and international transmission of H3N2 canine influenza a viruses from Korea during 2014-2017. *Journal of Veterinary Science* **24**, e78.

[46] **Lim S-I**, et al. (2022) Surveillance of canine influenza a virus in the Republic of Korea from 2016 to 2021. *Journal of the Preventive Veterinary Medicine* **46**, 183–188.

[47] **Chen M**, et al. (2023) Increased public health threat of avian-origin H3N2 influenza virus caused by its evolution in dogs. *eLife* **12**, e83470.

[48] **Li Y**, et al. (2021) Characterization of canine influenza virus a (H3N2) circulating in dogs in China from 2016 to 2018. *Viruses* **13**, 2279.

[49] **Lyu Y**, et al. (2019) Canine influenza virus a(H3N2) clade with antigenic variation, China, 2016-2017. *Emerging Infectious Diseases* **25**, 161–165.

[50] **Ou J**, et al. (2022) Isolation and genetic characterization of emerging H3N2 canine influenza virus in Guangdong Province, Southern China, 2018–2021. *Frontiers in Veterinary Science* **9**, 810855.

[51] LA County Department of Public Health. *H3N2 canine influenza in Los Angeles County.* (http://publichealth.lacounty.gov/vet/influenzacanineh3n2.htm). Accessed 10 May 2023.

[52] **Cori A**, et al. (2013) A new framework and software to estimate time-varying reproduction numbers during epidemics. *American Journal of Epidemiology* **178**, 1505–1512.

[53] **De Maio N**, et al. (2015) New routes to phylogeography: A Bayesian structured coalescent approximation. *PLoS Genetics* **11**, e1005421.

[54] **Dudas G**, et al. (2018) MERS-CoV spillover at the camel-human interface. *eLife* **7**, e31257.

[55] **Frost SDW and Volz EM** (2010) Viral phylodynamics and the search for an 'effective number of infections'. *Philosophical Transactions of the Royal Society of London. Series B, Biological Sciences* **365**, 1879–1890.

[56] **Westgeest KB**, et al. (2014) Genomewide analysis of reassortment and evolution of human influenza a(H3N2) viruses circulating between 1968 and 2011. *Journal of Virology* **88**, 2844–2857.

[57] **Weaver S**, et al. (2018) Datamonkey 2.0: A modern web application for characterizing selective and other evolutionary processes. *Molecular Biology and Evolution* **35**, 773–777.

[58] **Chauché C**, et al. (2018) Mammalian adaptation of an avian influenza a virus involves stepwise changes in NS1. *Journal of Virology* **92** , e01875–17.

[59] **Jackson D**, et al. (2008) A new influenza virus virulence determinant: The NS1 protein four C-terminal residues modulate pathogenicity. *Proceedings of the National Academy of Sciences of the United States of America* **105**, 4381–4386.

[60] **Li X**, et al. (2024) The PB2 I714S mutation influenced mammalian adaptation of the H3N2 canine influenza virus by interfering with nuclear import efficiency and RNP complex assembly. *Emerging Microbes & Infections* **13**, 2387439.

[61] **Staller E**, et al. (2024) Structures of H5N1 influenza polymerase with ANP32B reveal mechanisms of genome replication and host adaptation. *Nature Communications* **15**, 4123.

[62] **Liu L**, et al. (2024) The V223I substitution in hemagglutinin reduces the binding affinity to human-type receptors while enhancing the thermal stability of the H3N2 canine influenza virus. *Frontiers in Microbiology* **15**, 1442163.

[63] **Newbury S**, et al. (2016) Prolonged intermittent virus shedding during an outbreak of canine influenza a H3N2 virus infection in dogs in three Chicago area shelters: 16 cases (march to May 2015). *Journal of the American Veterinary Medical Association* **248**, 1022–1026.

[64] **Centers for Disease Control and Prevention** (2019) *Guidance Regarding Agency Interpretation of "Rabies-Free" as It Relates to the Importation of Dogs Into the United States*. p. 724–730. Report No.: 2019–00506.

[65] **Kavin K.** (2020) *Dog Adoptions and Sales Soar During the Pandemic. Washington Post.* 2020.

[66] **Pieracci EG**, et al. (2021) U.S. dog importations during the COVID-19 pandemic: Do we have an erupting problem? *PLoS One* **16**, e0254287.

[67] **United States Department of Agriculture** (2019) *Report on the Importation of Live Dogs into the United States*. United States Department of Agriculture, Report No.: USDA_DogImportReport6-25-2019.

[68] **Martinez-Sobrido L**, et al. (2020) Characterizing emerging canine H3 influenza viruses. *PLoS Pathogens* **16**, e1008409.

[69] **Herfst S**, et al. (2012) Airborne transmission of influenza a/H5N1 virus between ferrets. *Science (New York, N.Y.)* **336**, 1534–1541.

[70] **Imai M**, et al. (2012) Experimental adaptation of an influenza H5 HA confers respiratory droplet transmission to a reassortant H5 HA/H1N1 virus in ferrets. *Nature* **486**, 420–428.

[71] **Hill V**, et al. (2022) The origins and molecular evolution of SARS-CoV-2 lineage B.1.1.7 in the UK. *Virus Evolution* **8**, veac080.

[72] **Korber B**, et al. (2020) Tracking changes in SARS-CoV-2 spike: Evidence that D614G increases infectivity of the COVID-19 virus. *Cell* **182**, 812–827.e19.

[73] **McCrone JT**, et al. (2022) Context-specific emergence and growth of the SARS-CoV-2 Delta variant. *Nature* **610**, 154–160.

[74] **Viana R**, et al. (2022) Rapid epidemic expansion of the SARS-CoV-2 omicron variant in southern Africa. *Nature* **603**, 679–686.

[75] **Goldhill DH and Turner PE** (2014) The evolution of life history trade-offs in viruses. *Current Opinion in Virology* **8**, 79–84.

[76] **Kareinen L**, et al. (2024) Highly pathogenic avian influenza a(H5N1) virus infections on fur farms connected to mass mortalities of black-headed gulls, Finland. *Euro Surveillance: Bulletin Europeen Sur Les Maladies Transmissibles = European Communicable Disease Bulletin* **29**, 2400063.

[77] **Uyeki TM**, et al. (2024) Highly pathogenic avian influenza a(H5N1) virus infection in a dairy farm worker. *The New England Journal of Medicine*, Published online: 3 May 2024. doi:10.1056/NEJMc2405371.

[78] **Zhou P**, et al. (2022) Domestic poultry are not susceptible to avian-origin H3N2 subtype canine influenza a virus. *Veterinary Microbiology* **272**, 109501.

[79] **Mänz B**, et al. (2013) Pandemic influenza a viruses escape from restriction by human MxA through adaptive mutations in the nucleoprotein. *PLoS Pathogens* **9**, e1003279.

[80] **Pinto RM**, et al. (2023) BTN3A3 evasion promotes the zoonotic potential of influenza a viruses. *Nature* **619**, 338–347.

[81] **Shi Y**, et al. (2014) Enabling the 'host jump': Structural determinants of receptor-binding specificity in influenza a viruses. *Nature Reviews. Microbiology* **12**, 822–831.

[82] ***Summary of Neuraminidase (NA) Amino Acid Substitutions Associated With Reduced Inhibition by Neuraminidase Inhibitors (NAIs).*** World Health Organization (WHO), 2023 Mar, p. 1–13.

[83] **Jeoung H-Y**, et al. (2013) A novel canine influenza H3N2 virus isolated from cats in an animal shelter. *Veterinary Microbiology* **165**, 281–286.

[84] **Zhao J**, et al. (2021) Emergence and characterization of a novel reassortant canine influenza virus isolated from cats. *Pathogens (Basel, Switzerland)* **10**: 1320.

[85] **Zhou P**, et al. (2019) Serological evidence of H3N2 canine influenza virus infection among horses with dog exposure. *Transboundary and Emerging Diseases* **66**, 915–920.

[86] **Lowen AC** (2017) Constraints, drivers, and implications of influenza a virus reassortment. *Annual Review of Virology* **4**, 105–121.

[87] **Ma EJ**, et al. (2016) Reticulate evolution is favored in influenza niche switching. *Proceedings of the National Academy of Sciences of the United States of America* **113**, 5335–5339.

[88] **Chen Y**, et al. (2018) Emergence and evolution of novel Reassortant influenza a viruses in canines in southern China. *MBio* **9**, e00909–18.

[89] **Meng B**, et al. (2023) Emergence of a novel reassortant H3N6 canine influenza virus. *Frontiers in Microbiology* **14**, 1186869.

[90] **Na W**, et al. (2015) Viral dominance of reassortants between canine influenza H3N2 and pandemic (2009) H1N1 viruses from a naturally co-infected dog. *Virology Journal* **12**, 134.

[91] **Song D**, et al. (2012) A novel reassortant canine H3N1 influenza virus between pandemic H1N1 and canine H3N2 influenza viruses in Korea. *The Journal of General Virology* **93**, 551–554.

[92] **Brown JD**, et al. (2024) Antibodies to influenza a(H5N1) virus in hunting dogs retrieving wild fowl, Washington, USA. *Emerging Infectious Diseases* **30**, 1271–1274.

[93] **Moreno A**, et al. (2023) Asymptomatic infection with clade 2.3.4.4b highly pathogenic avian influenza a(H5N1) in carnivore pets, Italy, April 2023. *Euro Surveillance: Bulletin Europeen Sur Les Maladies Transmissibles = European Communicable Disease Bulletin* **28**, 2300441.

[94] **Rabalski L**, et al. (2023) Emergence and potential transmission route of avian influenza a (H5N1) virus in domestic cats in Poland, June 2023. *Euro Surveillance: Bulletin Europeen Sur Les Maladies Transmissibles = European Communicable Disease Bulletin* **28**, 2300390.

[95] **Sillman SJ**, et al. (2023) Naturally occurring highly pathogenic avian influenza virus H5N1 clade 2.3.4.4b infection in three domestic cats in North America during 2023. *Journal of Comparative Pathology* **205**, 17–23.

[96] **Tsui JL-H**, et al. (2023) Genomic assessment of invasion dynamics of SARS-CoV-2 omicron BA.1. *Science (New York, N.Y.)* **381**: 336–343.

[97] **Worobey M**, et al. (2020) The emergence of SARS-CoV-2 in Europe and North America. *Science (New York, N.Y.)* **370**, 564–570.

[98] **Zhou B**, et al. (2009) Single-reaction genomic amplification accelerates sequencing and vaccine production for classical and swine origin human influenza a viruses. *Journal of Virology* **83**, 10309–10313.

[99] **Martin DP**, et al. (2015) RDP4: Detection and analysis of recombination patterns in virus genomes. *Virus Evolution* **1**, vev003.

[100] **Edgar RC** (2004) MUSCLE: Multiple sequence alignment with high accuracy and high throughput. *Nucleic Acids Research* **32**, 1792–1797.

[101] **Guindon S**, et al. (2010) New algorithms and methods to estimate maximum-likelihood phylogenies: Assessing the performance of PhyML 3.0. *Systematic Biology* **59**, 307–321.

[102] **Trifinopoulos J**, et al. (2016) W-IQ-TREE: A fast online phylogenetic tool for maximum likelihood analysis. *Nucleic Acids Research* **44**, W232–W235.

[103] **Markin A**, et al. (2024) *Revealing reassortment in influenza A viruses with TreeSort.* bioRxiv.

[104] **Rambaut A**, et al. (2016) Exploring the temporal structure of heterochronous sequences using TempEst (formerly path-O-gen). *Virus Evolution* **2**, vew007.

[105] **Suchard MA**, et al. (2018) Bayesian phylogenetic and phylodynamic data integration using BEAST 1.10. *Virus Evolution* **4**: vey016.

[106] **Rambaut A**, et al. (2018) Posterior summarization in Bayesian phylogenetics using tracer 1.7. *Systematic Biology* **67**, 901–904.

[107] **Lemey P**, et al. (2009) Bayesian phylogeography finds its roots. *PLoS Computational Biology* **5**, e1000520.

[108] **Vaughan TG**, et al. Efficient Bayesian inference under the structured coalescent. *Bioinformatics* (Oxford, England) 2014; **30**: 2272–2279.

[109] **Drummond AJ**, et al. (2006) Relaxed phylogenetics and dating with confidence. *PLoS Biology* **4**, e88.

[110] **Minin VN**, **Bloomquist EW and Suchard MA** (2008) Smooth skyride through a rough skyline: Bayesian coalescent-based inference of population dynamics. *Molecular Biology and Evolution* **25**, 1459–1471.

[111] **Shapiro B**, **Rambaut A and Drummond AJ** (2006) Choosing appropriate substitution models for the phylogenetic analysis of protein-coding sequences. *Molecular Biology and Evolution* **23**, 7–9.

[112] **Bielejec F**, et al. (2016) SpreaD3: Interactive visualization of spatiotemporal history and trait evolutionary processes. *Molecular Biology and Evolution* **33**, 2167–2169.

[113] **Bouckaert R**, et al. (2019) BEAST 2.5: An advanced software platform for Bayesian evolutionary analysis. *PLoS Computational Biology* **15**, e1006650.